Journal of Biomechanics 42 (2009) 2061–2067

Contents lists available at ScienceDirect

Journal of Biomechanics

journal homepage: www.elsevier.com/locate/jbiomech
www.JBiomech.com

Specimen-specific multi-scale model for the anisotropic elastic constants of human cortical bone

Justin M. Deuerling, Weimin Yue [1], Alejandro A. Espinoza Orías [2], Ryan K. Roeder *

Department of Aerospace and Mechanical Engineering, University of Notre Dame, Notre Dame, IN 46556, United States

ARTICLE INFO

Article history:
Accepted 2 June 2009

Keywords:
Anisotropy
Compact bone
Cortical bone
Elastic constants
Micromechanical model
Multi-scale model
Orientation distribution function
Specimen-specific model

ABSTRACT

The anisotropic elastic constants of human cortical bone were predicted using a specimen-specific micromechanical model that accounted for structural parameters across multiple length scales. At the nano-scale, the elastic constants of the mineralized collagen fibril were estimated from measured volume fractions of the constituent phases, namely apatite crystals and Type I collagen. The elastic constants of the extracellular matrix (ECM) were predicted using the measured orientation distribution function (ODF) for the apatite crystals to average the contribution of misoriented mineralized collagen fibrils. Finally, the elastic constants of cortical bone tissue were determined by accounting for the measured volume fraction of Haversian porosity within the ECM. Model predictions using the measured apatite crystal ODF were not statistically different from experimental measurements for both the magnitude and anisotropy of elastic constants. In contrast, model predictions using common idealized assumptions of perfectly aligned or randomly oriented apatite crystals were significantly different from the experimental measurements. A sensitivity analysis indicated that the apatite crystal volume fraction and ODF were the most influential structural parameters affecting model predictions of the magnitude and anisotropy, respectively, of elastic constants.

1. Introduction

The elastic constants of human cortical bone are either transversely isotropic or orthotropic (Ashman et al., 1984), depending on the anatomic origin of the tissue (Espinoza Orías et al., 2009). Decreases in the magnitude of the elastic constants have been correlated with aging (Zioupos and Currey, 1998) and microdamage accumulation (Burr et al., 1998), as well as bone diseases such as osteoporosis (Hasegawa et al., 1995) and osteogenesis imperfecta (Mehta et al., 1999). Micromechanical models have been developed to investigate the structural origins of elastic inhomogeneity and anisotropy.

Micromechanical models have considered microstructural features, such as osteonal "fibers" embedded in a matrix of interstitial bone (Aoubiza et al., 1996; Dong and Guo, 2006; Hogan, 1992; Katz, 1980) or elongated Haversian porosity embedded within an isotropic extracellular matrix (ECM) (Currey and Zioupos, 2001; Sevostianov and Kachanov, 2000). These models predicted transversely isotropic elastic constants with magnitude dependent upon measurements or assumptions for the elastic constants and volume fraction of each phase (e.g., osteonal vs. interstitial bone). However, these models did not account for the role of the primary constituents of the ECM, namely apatite crystals and Type I collagen.

Other micromechanical models have focused on ultrastructural (nano-scale) features, treating mineralized collagen fibrils as an isotropic collagen matrix reinforced by aligned, elongated apatite crystals (Akiva et al., 1998; Akkus, 2005; Kotha and Guzelsu, 2007; Wagner and Weiner, 1992) or, alternatively, a randomly oriented apatite crystal foam reinforced by unidirectional collagen fibers (Aoubiza et al., 1996; Hellmich and Ulm, 2002; Hellmich et al., 2004). In either case, the predicted elastic behavior at the nano-scale is extended to the tissue level by assuming some orientation of the apatite crystals. The importance of the orientation of apatite crystals was first noted by Currey who proposed the use of fiber-reinforced composite models consisting of perfectly aligned apatite crystals embedded in a continuous isotropic collagen matrix (Currey, 1969). However, the model substantially overestimated and the elastic constants in the longitudinal and transverse direction, respectively, of human cortical bone. The approach was later refined by restricting the assumption of perfectly aligned apatite crystals to within a single lamella and then assigning an angle of misorientation relative to the longitudinal bone axis for alternating lamellae (Akiva et al., 1998; Wagner and Weiner, 1992). The angular dependence of the elastic modulus of human cortical bone was more accurately predicted,

* Corresponding author. Tel.: +574 631 7003; fax: +574 631 2144.
E-mail address: rroeder@nd.edu (R.K. Roeder).
[1] Current address: Granger Engineering, LLC, Granger, IN 46530, United States.
[2] Current address: Department of Orthopaedic Surgery, Rush University Medical Center, Chicago, IL 60612, United States.

0021-9290/$ - see front matter © 2009 Elsevier Ltd. All rights reserved.
doi:10.1016/j.jbiomech.2009.06.002

but the discrete orientations prescribed for the apatite crystals within each lamella were idealized.

The true distribution of apatite crystal orientations relative to the longitudinal bone axis can be measured by X-ray diffraction using quantitative texture analysis. The elongated *c*-axes of apatite crystals exhibit a preferred orientation in the longitudinal anatomic axis of long bones (Sasaki et al., 1989; Wenk and Heidelbach, 1999; Yue, 2006). A preferred orientation can be quantified by a measured orientation distribution function (ODF), which is a statistical function describing the relative probability for a volume of crystals having a given angle of misorientation (Bunge, 1985). Bundy (1985) proposed the use of an ODF as a weight function to average the contribution of a misoriented representative volume element (RVE) to determine the elastic constants of the ECM as a continuum. The effectiveness of this approach was recently demonstrated in a micromechanical model for synthetic hydroxyapatite whisker reinforced polymer biocomposites (Yue and Roeder, 2006).

In summary, micromechanical models for cortical bone have focused on either ultrastructural or microstructural features, but none have incorporated an accurate representation of the apatite crystal orientation distribution to connect the nano-scale and micro-scale behavior. Therefore, the objective of this study was to develop a micromechanical model that accounted for both ultrastructural and microstructural features to more accurately predict the anisotropic elastic constants of human cortical bone tissue (Fig. 1). Important structural parameters, including the apatite crystal ODF, were experimentally measured for human cortical bone specimens. The magnitude and anisotropy of elastic constants predicted by the micromechanical model were compared to experimental measurements from the same specimens. The sensitivity of model predictions to both measured and assumed structural parameters was also investigated, including a comparison of the measured apatite crystal ODF vs. common idealized assumptions.

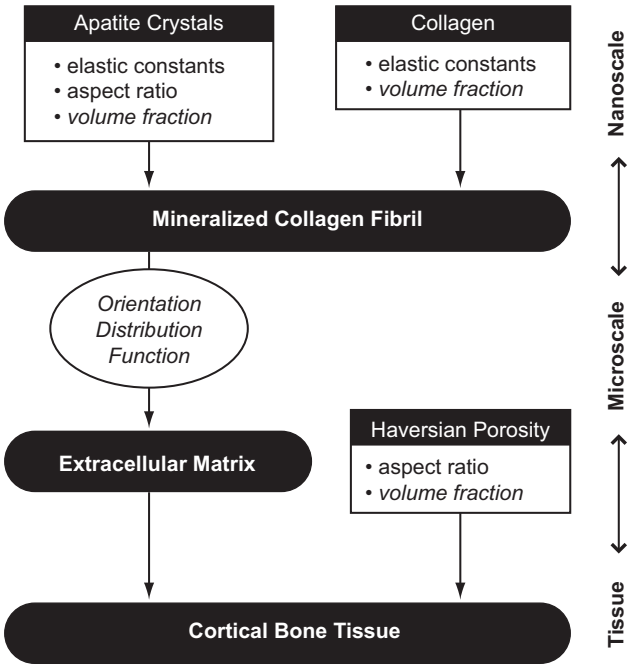

Fig. 1. Schematic diagram of the specimen-specific multi-scale model showing the structural features used to predict elastic constants at each of the three hierarchical levels. Features in *italics* indicate parameters that were experimentally measured for each specimen. All other parameters were estimated from mean values reported in the literature (Table 1).

2. Materials and methods

2.1. Specimen preparation

Twelve parallelepiped specimens (nominally $5\times5\times5$ mm) were machined from the femur of a 78-year-old Caucasian male donor presenting no toxicology or bone-related pathology. The specimens were sectioned from each of the four anatomic quadrants (anterior, medial, posterior, and lateral) at three locations along the femoral diaphysis (20%, 50%, and 85% of total femur length) to maximize variability in the structure and properties observed within a single femur (Espinoza Orías et al., 2009). An orthogonal curvilinear coordinate system with radial (1), circumferential (2), and longitudinal (3) axes was defined by the anatomic shape of the femoral diaphysis. Specimens were stored at −20 °C in a solution of 50% ethanol and 50% phosphate buffered saline during interim periods, and returned to a fully hydrated state for mechanical characterization.

2.2. Elastic constants

Elastic constants were measured for each specimen using an ultrasonic wave propagation technique described in detail elsewhere (Espinoza Orías et al., 2009). Briefly, longitudinal waves were propagated through the specimen along the three mutually orthogonal specimen axes. The stiffness coefficients, C_{11}, C_{22}, and C_{33}, were measured as

$$C_{ii} = \rho_{app} v_{ii}^2 \quad (i = 1,\ 2,\ 3) \tag{1}$$

where ρ_{app} is the apparent tissue density and v_{ii} is the longitudinal wave velocity in the i-th specimen direction. The apparent density of each specimen was measured as

$$\rho_{app} = \frac{M}{M-S}\rho_{H_2O} \tag{2}$$

where M is the mass of the bone specimen when fully saturated with deionized water, S the apparent mass when suspended in deionized water, and ρ_{H_2O} the density of deionized water (Ashman et al., 1984; ASTM, 1999). For specimens taken from the mid-diaphysis (50% of total femur length), elastic constants (mean ± standard deviation) measured in the radial, C_{11} (18.9 ± 2.7 GPa), and circumferential, C_{22} (19.3 ± 2.0 GPa), anatomic directions were not significantly different ($p = 0.83$, t-test) (Espinoza Orías et al., 2009). However, for specimens taken from locations near the epiphyses (20% and 85% of total femur length), C_{11} (12.9 ± 1.8 GPa) and C_{22} (19.0 ± 2.2 GPa) were significantly different ($p < 0.0005$, t-test). Therefore, the mean of the radial and circumferential elastic constants was defined as the transverse elastic constant to facilitate comparison to the transversely isotropic model predictions described below. Finally, an anisotropy ratio was defined as the ratio of the longitudinal and transverse elastic constants (Hasegawa et al., 1994; Turner et al., 1995).

2.3. Apatite crystal orientation distribution

The ODF for apatite crystals in the ECM of each specimen was measured by X-ray diffraction and quantitative texture analysis using methods described in detail elsewhere (Yue and Roeder, 2006; Yue, 2006). Briefly, specimen surfaces normal to the longitudinal anatomic axis were polished with a series of diamond compounds to a 3 μm final finish. Specimens were mounted on the goniometer of a General Area Detector Diffraction System (GADDS) equipped with a two-dimensional HI-STAR detector (Bruker AXS Inc., Madison, WI). Cu Kα radiation was generated at 40 kV and 40 mA and focused on the specimen by a 0.5 mm diameter pinhole collimator. A total of 72 two-dimensional X-ray diffraction spectra were collected at 5° rotations about the longitudinal bone axis for each of three crystallographic reflections (002, 222, and 213) for apatite. The ODF, $g(\theta)$, for each specimen (Fig. 2) was calculated from the pole figures for each reflection using the arbitrarily defined cells method (LaboTex, Version 2.1, LaboSoft s.c., Poland), after normalizing by a random powder sample prepared by grinding adjacent tissue.

2.4. Phase volume fractions

The specific gravity of the ECM of each specimen was measured as

$$\rho_{ECM} = \frac{D}{D-S}\rho_{H_2O} \tag{3}$$

where D is the dry mass, S the apparent mass when suspended in deionized water, and ρ_{H_2O} the density of deionized water (ASTM, 1999; Wang et al., 2001). After measuring the mass of each specimen while suspended in deionized water (S), the specimens were dehydrated by soaking in 70%, 80%, and 90% ethanol solutions for 1 h each and then in 100% ethanol for 8 h. After dehydration, specimens were dried in a vacuum oven at 90 °C for 8 h before measuring the dry mass (D). Linear interpolation was used to approximate the phase volume fractions based on values

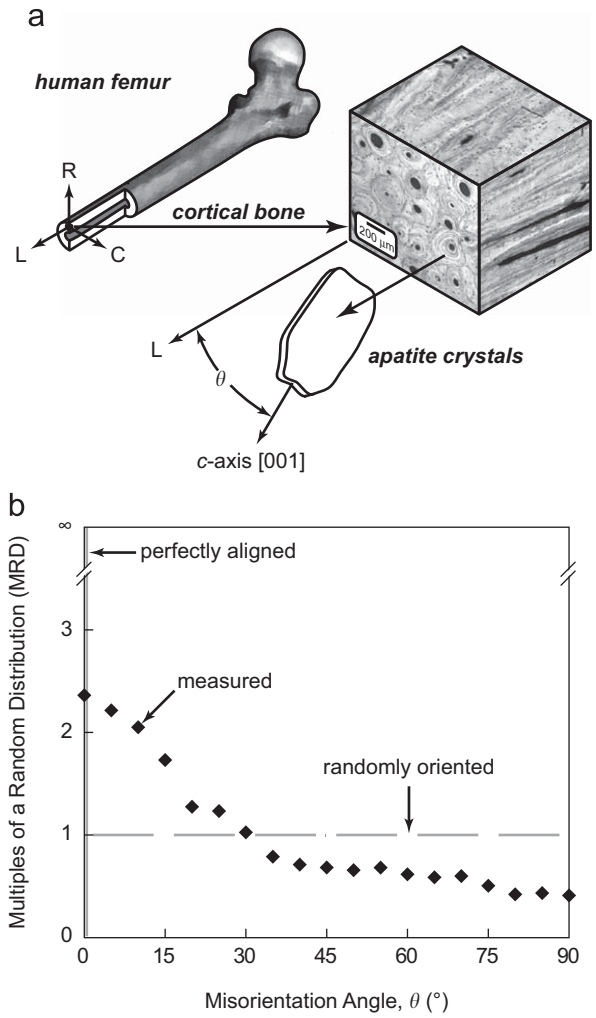

Fig. 2. (a) Schematic diagram showing the angle of misorientation (θ) between the longitudinal (L) bone axis and the elongated c-axis of an apatite crystal within a specimen prepared from the femoral diaphysis. (b) The measured orientation distribution function (ODF) for apatite crystals in a representative specimen, showing a c-axis (0 0 1) preferred orientation in the longitudinal (L) anatomic axis. Common idealized assumptions of perfectly aligned or randomly oriented apatite crystals are also shown schematically for comparison. Note that the degree of preferred orientation is shown in multiples of a random distribution (MRD), where MRD = 1 corresponds to random probability. For example, an orientation with MRD = 2.3 is 2.3 times more likely to occur than by random probability.

reported in the literature for the density of bone mineral, 2.86 g/cm^3, and collagen, 1.23 g/cm^3 (Black and Mattson, 1982).

The volume fraction of Haversian porosity in each specimen was measured using histomorphometry. Polished specimen cross-sections normal to the longitudinal anatomic axis were imaged using a reflected light microscope (Eclipse ME600, Nikon Instruments Inc., Melville, NY) at 50 × magnification. The volume fraction of porosity was measured as a pixel area fraction after thresholding digital grayscale images into binary images (ImageJ, National Institutes of Health).

2.5. Micromechanical model

Cortical bone tissue was modeled considering three distinct hierarchical levels of structure (Fig. 1). In the first level, the elastic constants of the mineralized collagen fibril were modeled using Halpin-Tsai equations for oriented discontinuous square fiber reinforcements (Halpin, 1992) in a RVE comprising apatite crystals within a continuous collagen matrix. The Halpin-Tsai equations accounted for the elastic constants and measured volume fractions of the apatite crystals and collagen, as well as the aspect ratio of the apatite crystals. The mean aspect ratio (length/thickness) of apatite crystals was taken as 20, based upon measurements in the literature (Eppel et al., 2001). The transversely isotropic elastic constants of apatite crystals and isotropic elastic constants of collagen were also assigned values reported in the literature (Table 1).

In the second level, the elastic constants of RVEs misaligned from the longitudinal anatomic axis were determined using tensor transformation laws. The effective elastic constants of the ECM were then calculated by averaging the weighted contribution of all misoriented RVEs by an experimentally measured ODF as

$$\overline{C}_{\mathrm{ECM}} = \frac{\int C_{\mathrm{RVE}}(\theta)\cdot g(\theta)\,d\theta}{\int g(\theta)\,d\theta} \tag{4}$$

where θ is the angle of misorientation between the longitudinal bone axis and the elongated c-axis of the apatite crystal, $g(\theta)$ is the ODF, and $C_{\mathrm{RVE}}(\theta)$ is the stiffness tensor computed for the misoriented RVE of a mineralized collagen fibril (cf., Bundy, 1985; Yue and Roeder, 2006).

In the third level of the model, the effective tissue properties were determined using the Halpin-Tsai equations to account for Haversian porosity within the ECM. The measured volume fraction of Haversian porosity was modeled as elongated voids, with a mean aspect ratio of 60 (Sevostianov and Kachanov, 2000), aligned parallel to the longitudinal bone axis.

Model predictions and experimentally measured elastic constants were plotted against the measured tissue porosity and compared using analysis of covariance (ANCOVA) (Statview 5.0.1, SAS Institute, Inc.). The measured anisotropy ratio was not correlated with the measured tissue porosity ($p = 0.82$, ANOVA). Therefore, the mean anisotropy ratio for model predictions and experimental measurements were compared using the Games-Howell post-hoc test for unequal variances. The level of significance for all tests was set at 0.05. In all cases, model predictions included the use of a measured ODF compared to idealized assumptions of randomly oriented or perfectly aligned apatite crystals (Fig. 2b). Finally, a sensitivity analysis was performed by adjusting model parameters (Fig. 1, Table 1) in 5% increments up to ±50% of their mean values to ascertain the relative effects of each structural parameter on the model predictions.

3. Results

Model predictions generated using experimentally measured ODFs for the apatite crystals compared favorably with the experimental measurements for both the longitudinal and transverse elastic constants (Fig. 3). Linear least squares regression of the model predictions, using the ODF, fell within the bounds of the 95% confidence interval for linear regression of the experimental data with tissue porosity. Moreover, linear regression coefficients for the experimental data and the model predictions, using the ODF, were not significantly different for either the longitudinal ($p = 0.90$, ANCOVA) or transverse elastic constants ($p = 0.09$, ANCOVA). In contrast, model predictions generated using assumptions of perfectly aligned or randomly oriented apatite crystals did not accurately predict the experimental elastic constants (Fig. 3). The assumption of perfectly aligned apatite crystals resulted in a statistically significant overestimation of longitudinal elastic constants and underestimation of transverse elastic constants ($p < 0.001$, ANCOVA). Conversely, the assumption of randomly oriented apatite crystals resulted in model predictions that underestimated the longitudinal elastic constant and overestimated the transverse elastic constant ($p < 0.001$, ANCOVA).

The experimentally measured anisotropy ratio was not significantly different from model predictions using the ODF (Table 2). In contrast, model predictions generated using assumptions of perfectly aligned or randomly oriented apatite crystals resulted in a statistically significant overestimation and underestimation, respectively, of the anisotropy ratio ($p < 0.05$, Games-Howell test).

Model predictions for the magnitude of the longitudinal and transverse elastic constants were most sensitive to the apatite crystal volume fraction and collagen elastic constants; moderately sensitive to the apatite crystal elastic constants and apatite crystal ODF; and relatively insensitive to the porosity volume fraction, apatite crystal aspect ratio, and porosity aspect ratio (Figs. 4a and b). However, model predictions for the elastic anisotropy were most sensitive to the apatite crystal ODF, moderately sensitive to a large increase in the apatite crystal volume fraction, and relatively insensitive to all other model parameters (Fig. 4c).

Table 1
Nano-scale and micro-scale structural and mechanical parameters used in the micromechanical model for the anisotropic elastic constants of human cortical bone.

Phase	Parameter	Value (s)	Reference
Apatite crystals	Elastic constants (transversely isotropic)	$C_{11} = 137$ GPa $C_{33} = 172$ GPa $C_{12} = 42.5$ GPa $C_{13} = 54.9$ Gpa $C_{44} = 39.6$ GPa	Katz and Ukraincik (1971)
	ODF	*Measured*	
	Volume fraction	*Measured*	
	Mean aspect ratio	*20*	Eppel et al. (2001)
Collagen	Elastic constants (isotropic)	$C_{11} = 3.9$ GPa $C_{12} = 1.1$ GPa	Sasaki and Odajima (1996)
	Volume fraction	*Measured*	
Haversian porosity	Aspect ratio	60	Sevostianov and Kachanov (2000)
	Volume fraction	*Measured*	

4. Discussion

The micromechanical model was able to predict the magnitude (Fig. 3) and anisotropy (Table 2) of elastic constants for femoral cortical bone specimens from a single donor. Model predictions were based on specimen-specific measurements of relevant structural parameters, including the apatite crystal ODF, the volume fraction of apatite crystals, and the volume fraction of Haversian porosity. The apatite crystal ODF was shown to be essential to the accuracy of the model predictions. Previous models have assumed either perfectly aligned (Currey, 1969; Kotha and Guzelsu, 2007) or randomly oriented (Hellmich and Ulm, 2002; Hellmich et al., 2004) apatite crystals, which were shown within the present model to result in inaccurate predictions (Fig. 3, Table 2). Other micromechanical models have achieved reasonable correlation with the elastic constants of cortical bone by assuming a specified angle of misorientation for parallel-fibered lamellae (Akiva et al., 1998, Aoubiza et al., 1996; Wagner and Weiner, 1992); however, the actual distribution of apatite crystal orientations is not limited to specific angles. Measured ODFs for apatite crystals in cortical bone exhibited preferred orientation in the longitudinal bone axis with a continuous decrease in probability with an increasing angle of misorientation (Fig. 2). Moreover, the apatite crystal ODF varies with the origin of the tissue (Wenk and Heidelbach, 1999; Yue, 2006). Thus, the apatite crystal ODF most accurately characterizes the organization of apatite crystals in the ECM.

The organization of the apatite crystals was also identified as the primary factor governing the elastic anisotropy of cortical bone (Table 2, Fig. 4c). The anisotropy ratio of human cortical bone was changed only slightly when deproteinized, but decreased significantly when demineralized, indicating that the mineral phase was responsible for the anisotropy (Hasegawa et al., 1994; Turner et al., 1995). Furthermore, the elastic anisotropy of cortical bone was recently shown to exhibit systematic variation with anatomic location (Espinoza Orías et al., 2009) which was correlated with tissue porosity and the apatite crystal ODF (Yue, 2006). Thus, the results of the present study provide a theoretical basis to explain and investigate the dependence of elastic anisotropy on the apatite crystal ODF.

The model incorporated structural information across multiple length scales in the prediction of tissue-level elastic constants. Previous models have assumed or measured the elastic constants of micro-scale structural features when predicting elastic constants at the tissue level (Dong and Guo, 2006; Hogan, 1992; Katz, 1980). For example, Dong and Guo (2006) predicted the elastic moduli of cortical bone using assumed properties and measured volume fractions for osteonal and interstitial bone. These models cannot alone account for variation in micro-scale properties, due to nano-scale changes in the organization and volume fraction of apatite crystals and collagen, e.g., hyper- or hypomineralization. In fact, the elastic constants of cortical bone have been shown to be highly dependent on the level of mineralization (Currey, 1988; Hernandez et al., 2001; Keller, 1994).

The sensitivity analysis (Fig. 4) revealed the relative influence of seven structural parameters (Table 1), occurring over multiple length scales (Fig. 1), on the prediction of tissue-level elastic constants and anisotropy using the micromechanical model with an ODF. The analysis was carried out to $\pm 50\%$ of the mean experimental or literature value for each structural parameter to consider the widest range of variation conceivable, while not violating any assumptions or boundary conditions in the model. Thus, Fig. 4 may be useful to compare relative changes in the magnitude and anisotropy of elastic constants due to changes in different structural parameters, *provided* that the amount of change in a given structural parameter can be justified based on experimental data. In other words, some of the effects shown in Fig. 4 may not be physiologically relevant. For example, a 50% change in the tissue porosity is quite possible, but a 50% change in the apatite elastic constants is unlikely, if not impossible. Thus, with proper care, the model could also be used to investigate complex, concomitant changes in structural parameters, e.g., associated with disease.

The multi-scale micromechanical model presented in this study was not without its own limitations. Several structural parameters were assumed and held constant using values reported in the literature. The sensitivity analysis indicated that two of these parameters, the elastic constants of collagen and apatite, were influential parameters affecting the magnitude of predicted elastic constants (Figs. 4a and b). However, the sensitivity of the model to these parameters is not entirely troublesome, since we are not aware of any experimental data showing significant specimen-to-specimen variation in the elastic constants of these fundamental phases. On the other hand, the accuracy of existing experimental measurements (Table 1) for the elastic constants of collagen and apatite is not known. The values of the other assumed structural parameters, the aspect ratio of the apatite crystals and Haversian porosity, likely vary from specimen-to-specimen. However, this potential weakness is minimized by results of the sensitivity analysis, which indicated that the aspect ratios had an insignificant effect on model predictions (Fig. 4).

Specimen-specific measurement of the apatite crystal volume fraction was dependent on an assumed density of the collagen and

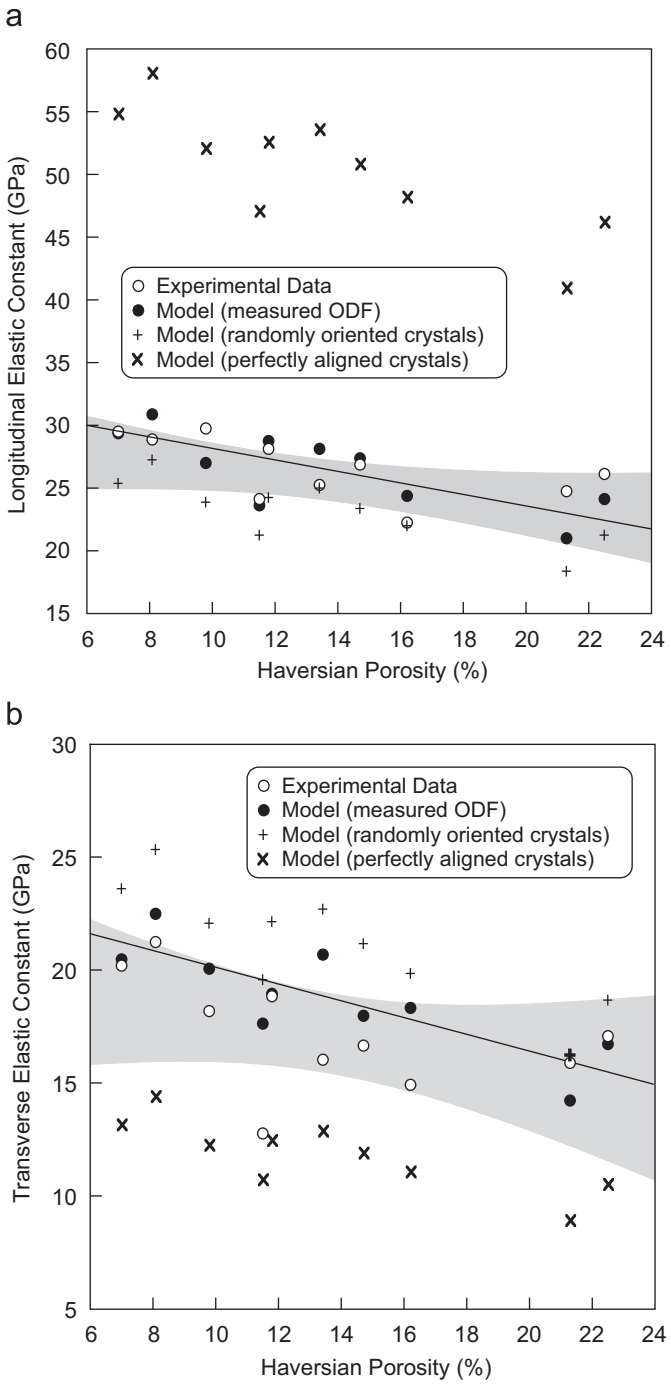

Fig. 3. Experimental measurements for (a) longitudinal and (b) transverse elastic constants compared to micromechanical model predictions using the measured ODF, as well as common idealized assumptions of randomly oriented or perfectly aligned apatite crystals. The shaded area shows the 95% confidence interval for linear least squares regression of the experimental elastic constants with the Haversian porosity. The solid line shows linear least squares regression of model predictions using the measured ODF with the Haversian porosity.

apatite phases. The density of collagen has been reported as 1.23 g/cm^3 (Black and Mattson, 1982), 1.28 g/cm^3 (Wang et al., 2001), and 1.41 g/cm^3 (Lees, 1987; Lees and Heeley, 1981), and the density of apatite bone mineral has been reported as 2.86 g/cm^3 (Black and Mattson, 1982), 3.00 g/cm^3 (Wang et al., 2001), and 3.15 g/cm^3 (Sudarsanan and Young, 1969). Thus, the measured mineral volume fractions used in the present model could vary by as much as 7% depending on the selected densities of collagen and

Table 2
The mean (± standard deviation) anisotropy ratio for the longitudinal and transverse elastic constants of all specimens from experimental measurements and model predictions.

	Anisotropy ratio
Experimental data	1.56 (0.14)
Model (measured ODF)	1.41 (0.07)
Model (randomly oriented crystals)	1.09 (0.02)
Model (perfectly aligned crystals)	4.27 (0.15)

The experimentally measured anisotropy ratio was not significantly different from model predictions using the ODF; all other pairwise comparisons between groups exhibited statistically significant differences ($p<0.05$, Games-Howell test).

apatite. The sensitivity analysis indicated that a change of this magnitude could significantly effect the predicted elastic constants (Figs. 4a and b), but would have negligible effect on the predicted anisotropy ratio (Fig. 4c).

Other simplifications made to structural parameters dictated that the elastic anisotropy was limited to transverse isotropy; however, human cortical bone is known to also exhibit orthotropy (Ashman et al., 1984; Espinoza Orías et al., 2009). First, the apatite crystal ODF was approximated as axisymmetric to require a single misorientation angle between the elongated *c*-axis of apatite crystals and the longitudinal anatomic axis. The same methods employed to measure the apatite crystal ODF can be used without this restriction in symmetry such that the misorientation of apatite crystals is characterized by three Euler angles (Bunge, 1985). In this case, Eq. (4) can be rewritten to average over the Euler angular space and calculate orthotropic elastic constants. Second, the morphology of apatite crystals was modeled as square fibers, while apatite crystals in bone are known to be elongated plates (Eppel et al., 2001; Weiner and Price, 1986). The present model could be readily adapted to incorporate a plate-like morphology by adding a second aspect ratio and using Halpin-Tsai equations for oriented discontinuous ribbon or lamella-shaped reinforcements (Halpin, 1992).

Finally, the human cortical bone specimens in this study were all taken from a single donor. The robustness of the model should be further examined using specimens taken from multiple donors, exhibiting variation due to age, gender, and disease-related structural dissimilarities. Nonetheless, this study demonstrated that specimen-specific micromechanical models may be useful in the study of these conditions, in which concomitant, deleterious changes in multiple structural parameters may adversely affect mechanical properties.

5. Conclusions

A specimen-specific multi-scale model was developed to predict the anisotropic elastic constants of human cortical bone tissue based upon seven relevant structural parameters. Model predictions generated using experimentally measured apatite crystal ODFs compared favorably with the experimental measurements, for both the longitudinal and transverse elastic constants, as well as the anisotropy ratio. In contrast, model predictions generated using common assumptions of perfectly aligned and randomly oriented apatite crystals did not accurately predict the measured elastic constants and anisotropy. The apatite crystal volume fraction and ODF were the most sensitive structural parameters affecting the predicted elastic constant magnitude and anisotropy ratio, respectively.

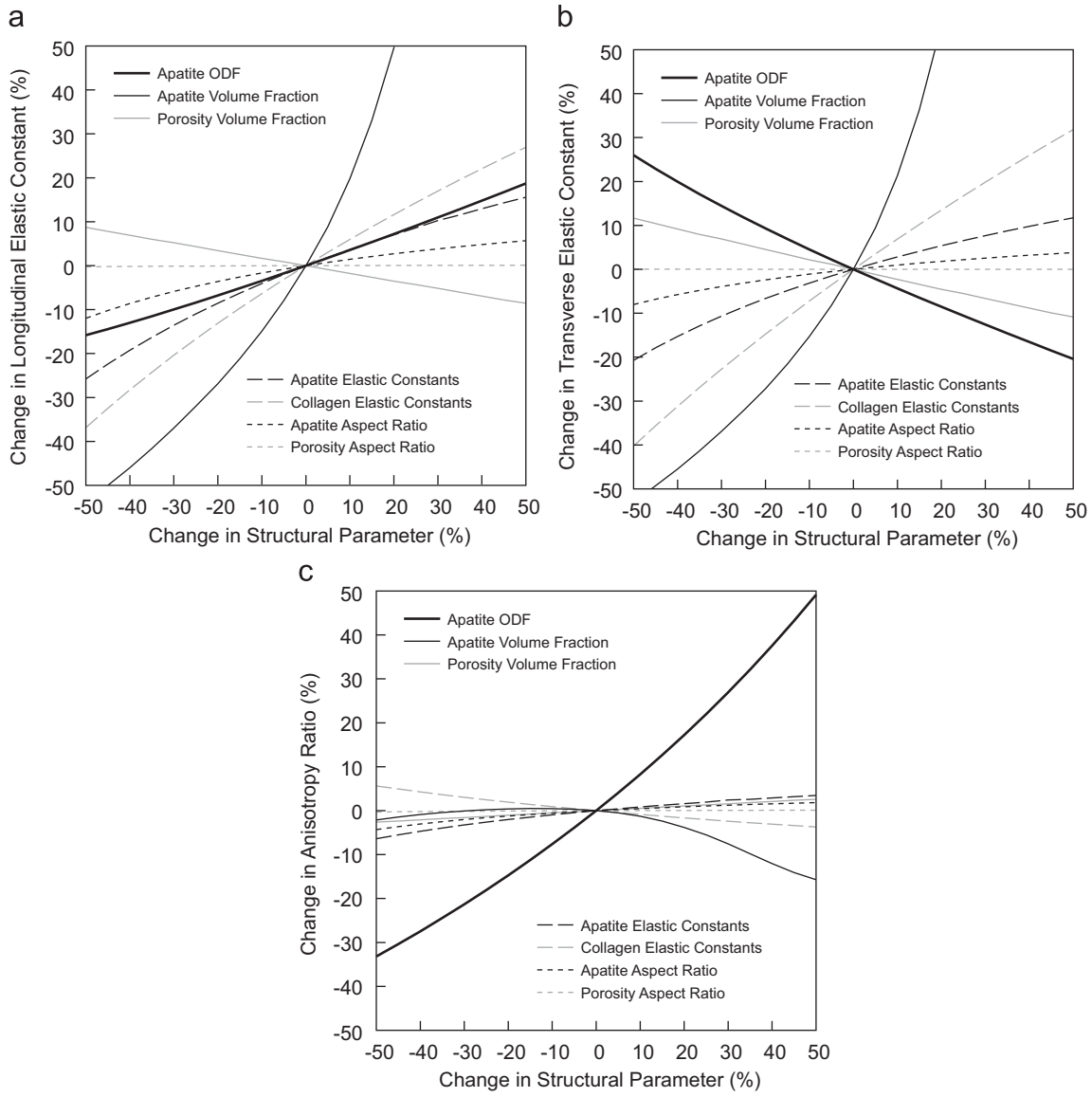

Fig. 4. Sensitivity analysis of the micromechanical model showing the relative effect of each structural parameter on the (a) longitudinal elastic constant, (b) transverse elastic constant, and the (c) anisotropy ratio for the longitudinal and transverse elastic constants.

Conflict of interest

I and my co-authors have no conflicts of interest to disclose regarding our submission entitled, "Specimen-specific multi-scale model for the anisotropic elastic constants of human cortical bone", for publication in the *Journal of Biomechanics.*

Acknowledgements

This research was partially supported by the Centers for Disease Control and Prevention (CE000789), the National Institutes of Health (AR049598) and the Indiana 21st Century Research and Technology Fund. The authors thank the Indiana University Medical School Anatomical Donations Program for providing the femur used in this study. The authors also thank Keith J. Bowman and Jacob Jones at Purdue University for providing training and use of the GADDS.

References

Akiva, U., Wagner, H.D., Weiner, S., 1998. Modelling the three-dimensional elastic constants of parallel-fibred and lamellar bone. Journal of Materials Science 33, 1497–1509.

Akkus, O., 2005. Elastic deformation of mineralized collagen fibrils: an equivalent inclusion-based composite model. Journal of Biomechanical Engineering 127, 383–390.

Aoubiza, B., Crolet, J.M., Meunier, A., 1996. On the mechanical characterization of compact bone structure using the homogenization theory. Journal of Biomechanics 29, 1539–1547.

Ashman, R.B., Cowin, S.C., Van Buskirk, W.C., Rice, J.C., 1984. A continuous wave technique for the measurement of the elastic properties of cortical bone. Journal of Biomechanics 17, 349–361.

ASTM Standard C373-88, 1999. Standard Test Method for Water Absorption, Bulk Density, Apparent Density and the Apparent Specific Gravity of Fired Whiteware Products. American Society for Testing Materials, West Conshohocken, PA.

Black, J., Mattson, R.U., 1982. Relationship between porosity and mineralization in the Haversian osteon. Calcified Tissue International 34, 332–336.

Bundy, K.J., 1985. Determination of mineral-organic bonding effectiveness in bone-theoretical considerations. Annals of Biomedical Engineering 13, 119–135.

Bunge, H.J., 1985. Representation of preferred orientations. In: Wenk, H.-R. (Ed.), Preferred Orientation in Deformed Metals and Rocks: An Introduction to Texture Analysis. Academic Press, Inc., Orlando, FL, pp. 73–108.

Burr, D.B., Turner, C.H., Naick, P., Forwood, M.R., Ambrosius, W., Hasan, M.S., Pidaparti, R., 1998. Does microdamage accumulation affect the mechanical properties of bone?. Journal of Biomechanics 31, 337–345.
Currey, J.D., 1969. The relationship between the stiffness and the mineral content of bone. Journal of Biomechanics 2, 477–480.
Currey, J.D., 1988. The effect of porosity and mineral content on the Young's modulus of elasticity of compact bone. Journal of Biomechanics 21, 131–139.
Currey, J.D., Zioupos, P., 2001. The effect of porous microstructure on the anisotropy of bone-like tissue: a counter example. Journal of Biomechanics 34, 707–708.
Dong, X.N., Guo, X.E., 2006. Prediction of cortical bone elastic constants by a two-level micromechanical model using a generalized self-consistent method. Journal of Biomechanical Engineering 128, 309–316.
Eppel, S.J., Tong, W., Katz, J.L., Kuhn, L., Glimcher, M.J., 2001. Shape and size of isolated bone mineralites measured using atomic force microscopy. Journal of Orthopaedic Research 19, 1027–1034.
Espinoza Orías, A.A., Renaud, J.E., Deuerling, J.M., Roeder, R.K., 2009. Anatomic variation in the elastic anisotropy of cortical bone tissue in the human femur. Journal of the Mechanical Behavior of Biomedical Materials 2, 255–263.
Halpin, J.C., 1992. Primer on Composite Materials Analysis. Technomic Publishing Co., Lancaster, PA.
Hasegawa, K., Turner, C.H., Burr, D.B., 1994. Contribution of collagen and mineral to the elastic anisotropy of bone. Calcified Tissue International 55, 381–386.
Hasegawa, K., Turner, C.H., Recker, R.R., Wu, E., Burr, D.B., 1995. Elastic properties of osteoporotic bone measured by scanning acoustic microscopy. Bone 16, 85–90.
Hellmich, C., Ulm, F.J., 2002. Are mineralized tissues open crystal foams reinforced by crosslinked collagen?. Journal of Biomechanics 35, 1199–1212.
Hellmich, C., Ulm, F.J., Dormieux, L., 2004. Can the diverse elastic properties of trabecular and cortical bone be attributed to only a few tissue-independent phase properties and their interactions?. Biomechanics and Modeling in Mechanobiology 2, 219–238.
Hernandez, C.J., Beaupré, G.S., Keller, T.S., Carter, D.R., 2001. The influence of bone volume fraction and ash fraction on bone strength and modulus. Bone 29, 74–78.
Hogan, H.A., 1992. Micromechanics modeling of Haversian cortical bone properties. Journal of Biomechanics 25, 549–556.
Katz, J.L., Ukraincik, K., 1971. On the anisotropic elastic properties of hydroxyapatite. Journal of Biomechanics 4, 221–227.
Katz, J.L., 1980. Anisotropy of Young's modulus of bone. Nature 283, 106–107.
Keller, T.S., 1994. Predicting the compressive mechanical behavior of bone. Journal of Biomechanics 27, 1159–1168.
Kotha, S.P., Guzelsu, N., 2007. Tensile behavior of cortical bone: dependence of organic material properties on bone mineral content. Journal of Biomechanics 40, 36–45.
Lees, S., 1987. Considerations regarding the structure of the mammalian mineralized osteoid from viewpoint of the generalized packing model. Connective Tissue Research 16, 281–303.
Lees, S., Heeley, J.D., 1981. Density of a sample bovine cortical bone matrix and its solid constituent in various media. Calcified Tissue International 33, 499–504.
Mehta, S.S., Antich, P.P., Landis, W.J., 1999. Bone material elasticity in a murine model of osteogenesis imperfecta. Connective Tissue Research 40, 189–198.
Sasaki, N., Matsushima, N., Ikawa, N., Yamamura, H., Fukuda, A., 1989. Orientation of bone mineral and its role in the anisotropic mechanical properties of bone-transverse anisotropy. Journal of Biomechanics 22, 157–164.
Sasaki, N., Odajima, S., 1996. Stress–strain curve and Young's modulus of a collagen molecule as determined by the X-ray diffraction technique. Journal of Biomechanics 29, 655–658.
Sevostianov, I., Kachanov, M., 2000. Impact of porous microstructure on the overall elastic properties of the osteonal cortical bone. Journal of Biomechanics 33, 881–888.
Sudarsanan, K., Young, R.A., 1969. Significant precision in crystal structural details: holly spring hydroxyapatite. Acta Crystallographica B 25, 1534–1543.
Turner, C.H., Chandran, A., Pidaparti, R.M.V., 1995. The anisotropy of osteonal bone and its ultrastructural implications. Bone 17, 85–89.
Wagner, H.D., Weiner, S., 1992. On the relationship between the microstructure of bone and its mechanical stiffness. Journal of Biomechanics 25, 1311–1320.
Wang, X., Bank, R.A., TeKoppele, J.M., Agrawal, C.M., 2001. The role of collagen in determining bone mechanical properties. Journal of Orthopaedic Research 19, 1021–1026.
Weiner, S., Price, P.A., 1986. Disaggregation of bone into crystals. Calcified Tissue International 39, 365–375.
Wenk, H.R., Heidelbach, F., 1999. Crystal alignment of carbonated apatite in bone and calcified tendon: results from quantitative texture analysis. Bone 24, 361–369.
Yue, W., 2006. Micromechanical Modeling of Hydroxyapatite Whisker Reinforced Polymer Composites and Cortical Bone Tissue. University of Notre Dame (Ph.D. Dissertation).
Yue, W., Roeder, R.K., 2006. Micromechanical model for hydroxyapatite whisker reinforced biocomposites. Journal of Materials Research 21, 2136–2145.
Zioupos, P., Currey, J.D., 1998. Changes in the stiffness, strength, and toughness of human cortical bone with age. Bone 22, 57–66.